ChemComm

ROYAL SOCIETY OF CHEMISTRY

COMMUNICATION

View Article Online
View Journal | View Issue

Check for updates

Cite this: *Chem. Commun.*, 2024, **60**, 4084

Received 19th January 2024,
Accepted 12th March 2024

DOI: 10.1039/d4cc00278d

rsc.li/chemcomm

Tetracene cyclophanes showing controlled intramolecular singlet fission by through-space orientations†

Hayato Sakai,[a] Keigo Nonaka,[b] Ryo Hayasaka,[a] Shakkeeb Thazhathethil,[b] Yoshimitsu Sagara *[bc] and Taku Hasobe *[a]

Tetracene cyclophanes: a series of cyclic tetracene dimers bridged by two flexible ethylene glycol units demonstrated enhanced intramolecular singlet fission through through-space orientations by suppressing the H-type excited complex.

Singlet fission (SF) is a spin-allowed multi-exciton generation process, in which a singlet exciton ($S_1 + S_0$) is converted into two individual triplet excitons ($T_1 + T_1$) through a correlated triplet pair (TT) in two nearby chromophores (eqn (1)).[1–4]

$$S_1 + S_0 \rightarrow TT \rightarrow T_1 + T_1 \quad (1)$$

Therefore, SF is highly promising for solar energy conversion. The energy matching conditions between the lowest singlet excited state and triplet excited state [$E(S_1) \geq 2E(T_1)$] are required for efficient SF. Acene derivatives are one of the typical SF molecules because they approximately satisfy the above conditions.[5] Many examples of covalently-bridged acyclic acene dimers for intramolecular SF (ISF) have been reported, so far.[6–19] We recently demonstrated the importance of a new structural parameter: ''conformational flexibility'', because the structural change from TT to $T_1 + T_1$ is required in addition to the conventional ''electronic coupling'' associated with the ISF rate constants.[5] In intramolecular reactions of covalently linked acyclic dimers (*e.g.*, ISF), it is generally difficult to achieve and control the dominant through-space interaction because the through-bond interaction is somehow mediated by the linker between the two chromophores. In contrast, in cyclic dimers, if the linker lengths between the two chromophores can be appropriately changed, the through-space interaction can become dominant and controllable. A few synthetic examples of cyclic pentacene dimers are reported (no example in the case of tetracene (Tet)),[20] whereas no one has yet focused on the linker length-dependent orientation control and ISF in such cyclic dimers.

Cyclophanes are cyclic compounds composed of aromatic and aliphatic groups.[21,22] The fascinating molecular structures have attracted much attention from the viewpoint of organic synthesis and supramolecular chemistry.[23] The control of through-space interactions between neighboring chromophores by cyclic structures is also useful for the occurrence of ISF. However, no attention has been drawn to the above concept.

Based on the above concept, the purpose of this study is to clarify the linker-distance dependent-ISF properties, which are dominated by the through-space interaction, using cyclic dimers. In this study, we synthesized tetracene cyclophanes: cyclic tetracene (Tet) dimers with two flexible ethylene glycol chains (denoted as $(Tet)_2$-CyO_n: n shows the number of oxygen atoms in ethylene glycol chains) together with the reference Tet monomer (Tet-ref) (Fig. 1). The detailed ISF properties associated with the linker length-dependent dimeric orientation are discussed.

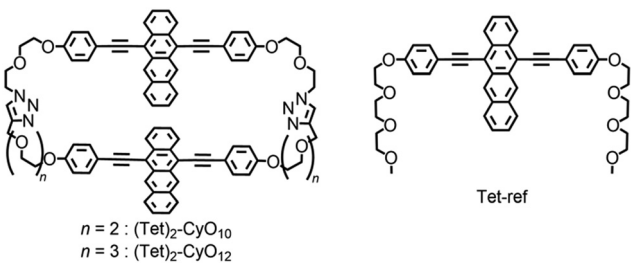

Fig. 1 Chemical structures of tetracene (Tet) cyclophanes and a reference compound in this study.

[a] Department of Chemistry, Faculty of Science and Technology, Keio University, Yokohama, Kanagawa 223-8522, Japan. E-mail: hasobe@chem.keio.ac.jp
[b] Department of Materials Science and Engineering, Tokyo Institute of Technology, Ookayama, Tokyo 152-8522, Japan. E-mail: sagara.y.aa@m.titech.ac.jp
[c] Living Systems Materialogy (LiSM) Research Group, International Research Frontiers Initiative (IRFI), Tokyo Institute of Technology, 4259 Nagatsuda-cho, Midori-ku, Yokohama, Kanagawa 226-8503, Japan

† Electronic supplementary information (ESI) available. Synthesis, spectroscopic and DFT calculations of the tetracene derivatives. See DOI: https://doi.org/10.1039/d4cc00278d

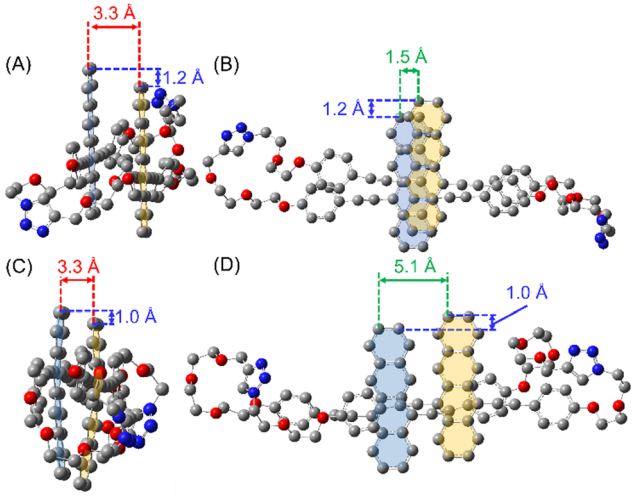

Fig. 2 Optimized structures of $(Tet)_2$-CyO_n calculated by DFT at the ωB97XD/DGTZVP level. (A) Side- and (B) top-views of $(Tet)_2$-CyO_{10} (cofacial orientation). (C) Side- and (D) top-views of $(Tet)_2$-CyO_{12} (slipping orientation). The oxygen and nitrogen atoms are highlighted in red and blue, respectively. The hydrogen atoms are omitted for simplicity.

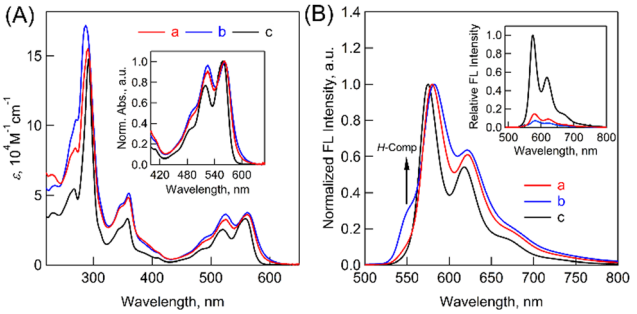

Fig. 3 (A) Absorption spectra of (a) $(Tet)_2$-CyO_{12} (red), (b) $(Tet)_2$-CyO_{10} (blue) and (c) Tet-ref (black) in THF. The inset shows the normalized spectra for comparison. (B) Normalized fluorescence spectra of (a) $(Tet)_2$-CyO_{12} (red), (b) $(Tet)_2$-CyO_{10} (blue) and (c) Tet-ref (black) in THF (λ_{ex} = 480 nm). The inset shows the comparison of the fluorescence intensities.

The synthetic procedures of $(Tet)_2$-CyO_n and Tet-ref are summarized in Schemes S1–S3 in the ESI.† The key step for the synthesis of $(Tet)_2$-CyO_{10} is a Cu(I)-catalyzed Huisgen cycloaddition between Tet derivatives carrying two oligoethylene glycols terminated with alkynes or azide groups based on our reported method.[24] $(Tet)_2$-CyO_{12} was similarly synthesized. The detailed synthetic procedures and characterizations are shown in Fig. S1–S54 in the ESI.†

To examine the structural configuration between the two Tet units in $(Tet)_2$-CyO_n, ^{1}H NMR was measured (Fig. S55 in ESI†) together with density functional theory (DFT) calculations at the ωB97XD/DGTZVP level (Fig. 2 and Fig. S56, S57 in ESI†). The proton signals derived from Tet and phenylacetylene substituents were seen in the spectral range of *ca.* 6.7–9.2 ppm. The up-field shifts of these proton peaks in $(Tet)_2$-CyO_n relative to Tet-ref were observed because of the effect of aromatic ring current from the other Tet unit. Moreover, the up-field shifted trend of $(Tet)_2$-CyO_{10} is much larger than that of $(Tet)_2$-CyO_{12}, which demonstrated the larger electronic coupling interaction between the two Tet units in $(Tet)_2$-CyO_{10}. DFT calculations also supported the plausible orientation between the two Tet units in $(Tet)_2$-CyO_n. In contrast with the approximate constant mean-plane distance between the two Tet units (3.3 Å), the slipping distances, namely the center-to-center distance of $(Tet)_2$-CyO_{12} (5.1 Å), significantly increased as compared to $(Tet)_2$-CyO_{10} (1.5 Å). The rotational barrier energies between the two Tet units by DFT demonstrated the smaller conformational flexibility of $(Tet)_2$-CyO_{10} due to the much larger energy barrier (Fig. S58 in ESI†).[7] Consequently, $(Tet)_2$-CyO_{10} shows large electronic coupling and small conformational flexibility, which is in sharp contrast with the small electronic coupling and large conformational flexibility observed in $(Tet)_2$-CyO_{12}.[5]

To further examine the electronic structures, steady-state absorption and fluorescence spectra of $(Tet)_2$-CyO_n were measured in THF. In absorption measurements (Fig. 3A), $(Tet)_2$-CyO_n demonstrated broadened spectra in the range from the UV to visible region (up to *ca.* 620 nm) as compared to Tet-ref. Additionally, the relative ratio of 0-1 to 0-0 vibronic progressions of the lowest-energy absorption band ($\varepsilon_{0\text{-}1}/\varepsilon_{0\text{-}0}$) was evaluated because it is a typical evaluation method for the coupling strength in molecular dimers.[25] Increased values of $(Tet)_2$-CyO_{12} (0.91) and $(Tet)_2$-CyO_{10} (0.97) were observed as compared to Tet-ref (0.77), whereas smaller interchromophore electronic coupling in $(Tet)_2$-CyO_{12} relative to $(Tet)_2$-CyO_{10} was observed. This agrees well with the above discussions in ^{1}H NMR and DFT calculations.

Then, fluorescence measurements demonstrated strong fluorescence quenching of $(Tet)_2$-CyO_n relative to Tet-ref together with the broadened spectra because of the dimeric form, which indicates a possibility of ISF in $(Tet)_2$-CyO_n (Fig. 3B and Table S1 in ESI†). Furthermore, the fluorescence quenching trend of $(Tet)_2$-CyO_{10} is larger than that of $(Tet)_2$-CyO_{12} because of the larger electronic coupling of $(Tet)_2$-CyO_{10} as stated above. Interestingly, an additional vibronic band was only observed in $(Tet)_2$-CyO_{10} at *ca.* 550 nm in the shorter wavelength region (Fig. 3B and 4), rather than the excimer observed in the longer wavelength region. This is probably attributable to the H-type excited complex (H-Comp) between two Tet units. A similar emission trend was observed in 9,10-bis(phenylethynyl)anthracene cyclophanes by us.[26,27] The excitation wavelength-dependent fluorescence spectra of $(Tet)_2$-CyO_{10} also demonstrated relatively larger emission derived from H-Comp at shorter excitation wavelengths (Fig. S59 in ESI†). In contrast with two different fluorescence lifetime components of $(Tet)_2$-CyO_{12}, which correspond to ISF and reverse triplet–triplet annihilation (TTA), the third lifetime species should be attributable to the emission of H-Comp in $(Tet)_2$-CyO_{10} (Fig. 4B and Table S2 in the ESI†).

To examine the dynamics of $(Tet)_2$-CyO_n, we have performed transient absorption measurements in THF. Before starting the detailed discussion, first, we assigned the singlet and triplet absorption spectra of the Tet unit (Fig. S60–S64 in ESI†). In the case of the singlet absorption, we employed Tet-ref and observed two different positive absorption bands (400–500 and

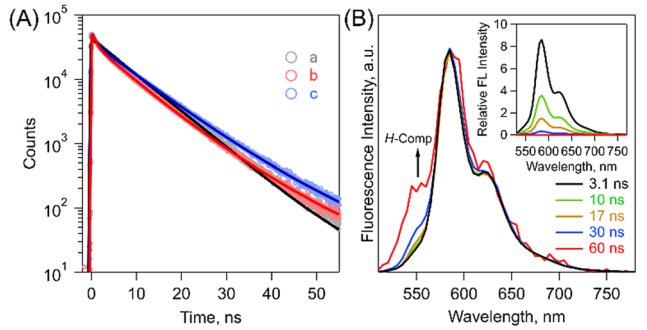

Fig. 4 (A) Fluorescence decay profiles of (a) Tet-ref (gray), (b) $(Tet)_2$-CyO_{10} (blue) and (c) $(Tet)_2$-CyO_{12} (red) in THF (λ_{ex} = 404 nm). The obtained lifetimes are summarized in Table S2 in the ESI.† (B) Normalized time-resolved emission spectra of $(Tet)_2$-CyO_{10} in THF (λ_{ex} = 404 nm). The inset shows the time-resolved emission spectra (λ_{ex} = 404 nm). 3.1 ns (black), 10 ns (green), 17 ns (brown), 30 ns (blue) and 60 ns (red).

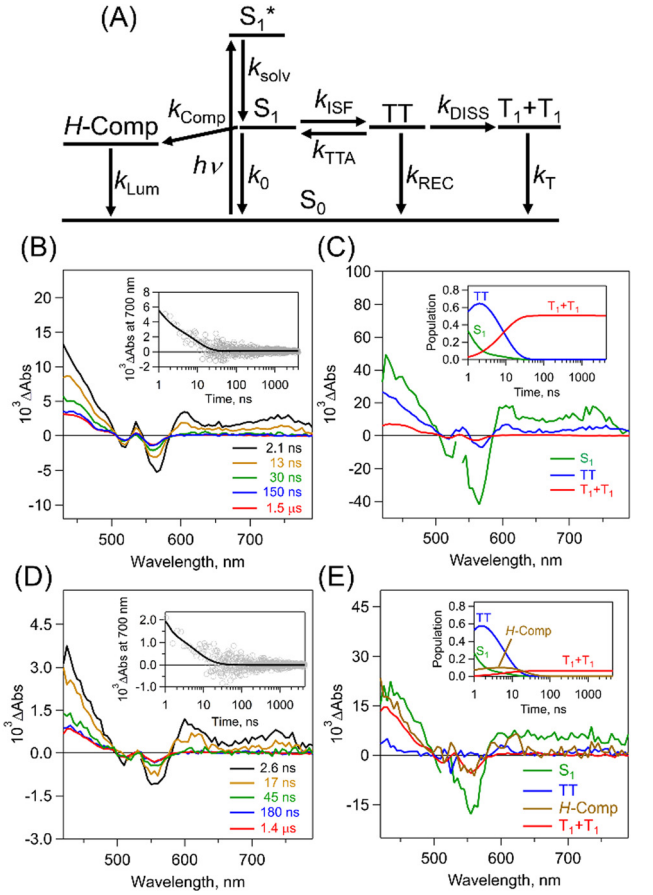

Fig. 5 (A) A proposed kinetic model. (B) ps-TAS of $(Tet)_2$-CyO_{12} in THF (λ_{ex}: 532 nm). The inset figure shows the time profile at 700 nm. (C) SAS of $(Tet)_2$-CyO_{12}: S_1 (black), TT (blue) and T_1 + T_1 (red). The inset shows the time-dependent population profiles. (D) ps-TAS of $(Tet)_2$-CyO_{10} in THF (λ_{ex}: 532 nm). The inset shows the time profile at 700 nm. (E) SAS of $(Tet)_2$-CyO_{10}: S_1 (black), TT (blue), H-Comp (brown) and T_1 + T_1 (red). The inset shows the time-dependent population profiles.

600–750 nm regions). In the triplet absorption, we employed triplet–triplet energy transfer from anthracene (a sensitizer) to $(Tet)_2$-CyO_n. The resulting individual triplet spectra were observed mainly in the range of *ca.* 400–500 nm. Note that the individual triplet absorption at wavelengths longer than 600 nm has quite small molar absorption coefficients, which is a major difference from the singlet absorption. Additionally, the molar absorption coefficients of these triplet spectra (ε_T) were determined to estimate individual triplet yields (Φ_T) (Tables S3–S6 in ESI†).

Then, we measured the femtosecond transient absorption spectra (fs-TAS) of $(Tet)_2$-CyO_n in THF (Fig. S65, S66 in ESI†). Typically, Fig. S66 in the ESI† shows fs-TAS of $(Tet)_2$-CyO_{12} and corresponding species-associated spectra (SAS) by target analysis (*vide infra*), respectively. After photoexcitation at 515 nm, initial singlet absorption bands of $(Tet)_2$-CyO_{12} appeared immediately, and then solvent relaxation occurred in the time region up to *ca.* 10 ps. Then, the two distinct singlet absorption band intensities in the short and long wavelength regions decreased, resulting in the formation of a correlated triplet pair (TT) at around 1 ns. In contrast, the photophysical behavior of $(Tet)_2$-CyO_{10} is roughly similar to that of $(Tet)_2$-CyO_{12}, whereas the above-mentioned deactivation process based on the H-Comp formation was included. Such spectral changes are in sharp contrast with Tet-ref.

To quantitatively and kinetically discuss the detailed photodynamics, we proposed a kinetic model for the occurrence of ISF and analyzed SAS (Fig. 5A and Scheme S4 in ESI†). The rate constant of the initial solvent relaxation process from the initial singlet excited state (S_1^*) to the solvent-relaxed singlet excited state (S_1) is denoted as k_{solv}. Then, the ISF from S_1 to TT (k_{ISF}) together with the deactivation from S_1 to the ground state (k_0), TTA (k_{TTA}), and deactivation and emission processes by H-Comp (k_{Comp} and k_{Lum}) are included. In addition to the direct recombination (k_{REC}) from TT to the ground state and deactivation process (k_T) from the T_1 + T_1 to the ground state, the TT can generate the T_1 + T_1 by the dissociation (k_{DISS}). SAS and corresponding time-dependent concentration profiles were obtained by target analysis.[28] The changes of the spectral shapes should be emphasized when comparing the SAS of fs-TAS in $(Tet)_2$-CyO_n (Fig. S65, S66 in ESI†). In particular, the maximum wavelength at around 400–500 nm changes from 426 nm (S_1^*) to 431 nm (S_1) and 432 nm (TT). Then, the obtained rate constants and quantum yields of TT (Φ_{TT}) and T_1 + T_1 (Φ_T) were summarized (Table 1). The k_{ISF} of $(Tet)_2$-CyO_{10} (1.5×10^9 s^{-1}) is larger than that of $(Tet)_2$-CyO_{12} (1.1×10^9 s^{-1}) because of the lager electronic coupling of $(Tet)_2$-CyO_{10}. These k_{ISF} values are an order of magnitude greater than k_{TTA}, k_0 and k_{Comp}, resulting in efficient ISF (Φ_{TT}: 65% for $(Tet)_2$-CyO_{10} and Φ_{TT}: 69% for $(Tet)_2$-CyO_{12}). Note the maximum Φ_{TT} is 100%. The larger kinetic ratios of k_{ISF} relative to k_{TTA} are consistent with the Φ_{TT} values. The k_{Comp} of $(Tet)_2$-CyO_{10} has a great effect on the decrease of the Φ_T (*vide infra*).

To further investigate the TT dissociation, picosecond transient absorption spectra (ps-TAS) of $(Tet)_2$-CyO_n were measured in THF with 532 nm excitation (Fig. 5B–E). The transient spectrum derived from TT (blue in Fig. 5B) initially appeared and the T_1 + T_1 were seen in both $(Tet)_2$-CyO_{10} and $(Tet)_2$-CyO_{12},

Table 1 Summarized kinetic parameter

	k_{solv},[a] 10^{10} s^{-1}	k_0,[b] 10^8 s^{-1}	k_{Comp},[a] 10^8 s^{-1}	k_{Lum},[c] 10^7 s^{-1}	k_{ISF},[a] 10^9 s^{-1}	k_{TTA},[a] 10^8 s^{-1}	k_{REC},[d] 10^7 s^{-1}	k_{DISS},[e] 10^7 s^{-1}	k_{ISF}/k_{TTA} (k_{DISS}/k_{REC})	k_T, 10^3 s^{-1} (τ_T, ms)	Φ_{TT},[h] %	Φ_T,[i] %
$(Tet)_2$-CyO_{10}	3.3	1.3	4.5	6.7	1.5	1.7	14	1.4	8.8 (0.10)	5.4[f] (0.19[f])	65	14 ± 1.2
$(Tet)_2$-CyO_{12}	8.8	1.3	—	—	1.1	1.1	6.1	5.7	10 (0.93)	5.5[f] (0.19[f])	69	108 ± 2.5
Tet-ref	1.2	1.3	—	—	—	—	—	—		5.1[g] (0.20[g])	—	0.8 ± 0.3

[a] Estimated by target analysis of fs-TAS. [b] Calculated by $k_0 = (\tau_S)^{-1}$, τ_S was estimated by fluorescence lifetime of Tet-ref (τ_S: 7.6 ns). [c] Calculated by $k_{Lum} = (\tau_{Lum})^{-1}$, τ_{Lum} was estimated by fluorescence lifetime of $(Tet)_2$-CyO_{10} (τ_{Lum}: 15.2 ns). [d] Calculated by $k_{REC} = k_{TT} - k_{DISS} = (\tau_{TT})^{-1} - k_{DISS}$, τ_{TT} was estimated by target analysis of ps-TAS. [e] Calculated by $k_{DISS} = k_{TT} \times \Phi_T/(2\Phi_{TT})$. [f] Calculated by $k_T = \tau_T^{-1}$, τ_T was estimated by ns-TAS. [g] Calculated by $k_T = (\tau_T)^{-1}$, τ_T was estimated by the sensitization experiment of Tet-ref. [h] Estimated by the population of TT considering k_{TTA} (Fig. 4C and E and Fig. S65, S66 in ESI). [i] Estimated by ps-TAS.

which agrees well with the above-mentioned triplet spectra of $(Tet)_2$-CyO_n by sensitization (Fig. S64 in ESI†). The k_{DISS} of $(Tet)_2$-CyO_{12} (5.7×10^7 s^{-1}) is much larger than that of $(Tet)_2$-CyO_{10} (1.4×10^7 s^{-1}), whereas the k_{REC} of $(Tet)_2$-CyO_{12} (6.1×10^7 s^{-1}) is smaller than that of $(Tet)_2$-CyO_{10} (1.4×10^8 s^{-1}).

Therefore, the relative ratio between k_{REC} and k_{DISS} (k_{DISS}/k_{REC}) in $(Tet)_2$-CyO_{12} (0.93) is significantly larger than $(Tet)_2$-CyO_{10} (0.10), indicating the accelerated TT dissociation in $(Tet)_2$-CyO_{12}. This is also associated with the much larger Φ_T in $(Tet)_2$-CyO_{12} (108%) relative to $(Tet)_2$-CyO_{10} (14%) (maximum Φ_T: 200%). The significant increase in Φ_T of $(Tet)_2$-CyO_{12} should be related to the suppression of H-Comp formation caused by the larger conformational flexibility because of the longer ethylene glycol chains.[5] The k_T was calculated from the lifetime (τ_T: 0.19 ms) by nanosecond transient absorption spectra in THF (Fig. S67, S68 in ESI†), as shown in Table 1. Additionally, fs-/ps-TAS of $(Tet)_2$-CyO_n in toluene (less-polar solvent) demonstrated the decreased Φ_{TT} and Φ_T in toluene relative to those in THF (Fig. S69–S72 and Tables S7, S8 in ESI†). The polar ethylene glycol chains are likely to be less structurally flexible in a less-polar solvent, preventing the TT dissociation.

In conclusion, a series of tetracene cyclophanes demonstrated the enhanced ISF by controlled through-space orientations. $(Tet)_2$-CyO_{12} exhibited the much-enhanced Φ_T (108%) as compared to $(Tet)_2$-CyO_{10} (14%) because of the suppression of H-Comp formation. Although the obtained Φ_T are not as high as those of reported acyclic Tet dimers with the highly efficient or quantitative Φ_T,[7,14,15,17] our synthetic strategy utilizing cyclophanes should provide new functionalization of SF.

This work was partially supported by JSPS KAKENHI Grant-in-Aid for Transformative Research Areas, ''Materials Science of Meso-Hierarchy'' (JP23H04876 to T. H., JP23H04878 to Y. S.) and ''Aquatic Functional Materials'' (JP20H05234 to T. H. and JP20H05198 to Y. S.).

Conflicts of interest

There are no conflicts to declare.

Notes and references

1 M. B. Smith and J. Michl, *Chem. Rev.*, 2010, **110**, 6891–6936.
2 K. Miyata, F. S. Conrad-Burton, F. L. Geyer and X. Y. Zhu, *Chem. Rev.*, 2019, **119**, 4261–4292.
3 R. Casillas, I. Papadopoulos, T. Ullrich, D. Thiel, A. Kunzmann and D. M. Guldi, *Energy Environ. Sci.*, 2020, **13**, 2741–2804.
4 R. M. Young and M. R. Wasielewski, *Acc. Chem. Res.*, 2020, **53**, 1957–1968.
5 T. Hasobe, S. Nakamura, N. V. Tkachenko and Y. Kobori, *ACS Energy Lett.*, 2022, **7**, 390–400.
6 H. Sakai, R. Inaya, H. Nagashima, S. Nakamura, Y. Kobori, N. V. Tkachenko and T. Hasobe, *J. Phys. Chem. Lett.*, 2018, **9**, 3354–3360.
7 S. Nakamura, H. Sakai, H. Nagashima, M. Fuki, K. Onishi, R. Khan, Y. Kobori, N. V. Tkachenko and T. Hasobe, *J. Phys. Chem. C*, 2021, **125**, 18287–18296.
8 S. Nakamura, H. Sakai, M. Fuki, Y. Kobori, N. V. Tkachenko and T. Hasobe, *J. Phys. Chem. Lett.*, 2021, **12**, 6457–6463.
9 S. Lukman, K. Chen, J. M. Hodgkiss, D. H. P. Turban, N. D. M. Hine, S. Dong, J. Wu, N. C. Greenham and A. J. Musser, *Nat. Commun.*, 2016, **7**, 13622.
10 S. N. Sanders, E. Kumarasamy, A. B. Pun, M. T. Trinh, B. Choi, J. Xia, E. J. Taffet, J. Z. Low, J. R. Miller, X. Roy, X. Y. Zhu, M. L. Steigerwald, M. Y. Sfeir and L. M. Campos, *J. Am. Chem. Soc.*, 2015, **137**, 8965–8972.
11 S. Nakamura, H. Sakai, M. Fuki, R. Ooie, F. Ishiwari, A. Saeki, N. V. Tkachenko, Y. Kobori and T. Hasobe, *Angew. Chem., Int. Ed.*, 2023, **62**, e202217704.
12 T. Kinoshita, S. Nakamura, M. Harada, T. Hasobe and G. Fukuhara, *Chem. Sci.*, 2023, **14**, 3293–3301.
13 J. Kim, H. T. Teo, Y. Hong, Y. C. Liau, D. Yim, Y. Han, J. Oh, H. Kim, C. Chi and D. Kim, *J. Am. Chem. Soc.*, 2023, **145**, 19812–19823.
14 T. Wang, H. Liu, X. Wang, L. Tang, J. Zhou, X. Song, L. Lv, W. Chen, Y. Chen and X. Li, *J. Mater. Chem. A*, 2023, **11**, 8515–8539.
15 N. V. Korovina, J. Joy, X. Feng, C. Feltenberger, A. I. Krylov, S. E. Bradforth and M. E. Thompson, *J. Am. Chem. Soc.*, 2018, **140**, 10179–10190.
16 Z. Wang, H. Liu, X. Xie, C. Zhang, R. Wang, L. Chen, Y. Xu, H. Ma, W. Fang, Y. Yao, H. Sang, X. Wang, X. Li and M. Xiao, *Nat. Chem.*, 2021, **13**, 559–567.
17 Y. Bo, Y. Hou, D. Thiel, R. Weiß, T. Clark, M. J. Ferguson, R. R. Tykwinski and D. M. Guldi, *J. Am. Chem. Soc.*, 2023, **145**, 18260–18275.
18 K. Majumder, S. Mukherjee, N. A. Panjwani, J. Lee, R. Bittl, W. Kim, S. Patil and A. J. Musser, *J. Am. Chem. Soc.*, 2023, **145**, 20883–20896.
19 C. Hetzer, D. M. Guldi and R. R. Tykwinski, *Chem. – Eur. J.*, 2018, **24**, 8245–8257.
20 H. M. Bergman, G. R. Kiel, R. J. Witzke, D. P. Nenon, A. M. Schwartzberg, Y. Liu and T. D. Tilley, *J. Am. Chem. Soc.*, 2020, **142**, 19850–19855.
21 Y. Morisaki, K. Inoshita and Y. Chujo, *Chem. – Eur. J.*, 2014, **20**, 8386–8390.
22 W. Kim, A. Nowak-Król, Y. Hong, F. Schlosser, F. Würthner and D. Kim, *J. Phys. Chem. Lett.*, 2019, **10**, 1919–1927.
23 D. Ramaiah, P. P. Neelakandan, A. K. Nair and R. R. Avirah, *Chem. Soc. Rev.*, 2010, **39**, 4158–4168.
24 S. Thazhathethil, T. Muramatsu, N. Tamaoki, C. Weder and Y. Sagara, *Angew. Chem., Int. Ed.*, 2022, **61**, e202209225.
25 H. Horinouchi, H. Sakai, Y. Araki, T. Sakanoue, T. Takenobu, T. Wada, N. V. Tkachenko and T. Hasobe, *Chem. – Eur. J.*, 2016, **22**, 9631–9641.
26 Y. Sagara, C. Weder and N. Tamaoki, *RSC Adv.*, 2016, **6**, 80408–80414.
27 Y. Sagara, Y. C. Simon, N. Tamaoki and C. Weder, *Chem. Commun.*, 2016, **52**, 5694–5697.
28 J. J. Snellenburg, S. Laptenok, R. Seger, K. M. Mullen and I. H. M. van Stokkum, *J. Stat. Softw.*, 2012, **49**, 1–22.